



Massive spectral data analysis for plant breeding using parSketch-PLSDA method: Discrimination of sunflower genotypes

Maxime Ryckewaert, Maxime Metz, Daphné Héran, Pierre George, Bruno Grèzes-Besset, Reza Akbarinia, Jean Michel Roger, Ryad Bendoula

► To cite this version:

Maxime Ryckewaert, Maxime Metz, Daphné Héran, Pierre George, Bruno Grèzes-Besset, et al.. Massive spectral data analysis for plant breeding using parSketch-PLSDA method: Discrimination of sunflower genotypes. Biosystems Engineering, 2021, 210, pp.69-77. 10.1016/j.biosystemseng.2021.08.005 . hal-03329674

HAL Id: hal-03329674

<https://hal.inrae.fr/hal-03329674>

Submitted on 7 Jun 2022

HAL is a multi-disciplinary open access archive for the deposit and dissemination of scientific research documents, whether they are published or not. The documents may come from teaching and research institutions in France or abroad, or from public or private research centers.

L'archive ouverte pluridisciplinaire **HAL**, est destinée au dépôt et à la diffusion de documents scientifiques de niveau recherche, publiés ou non, émanant des établissements d'enseignement et de recherche français ou étrangers, des laboratoires publics ou privés.



Distributed under a Creative Commons Attribution - NonCommercial - NoDerivatives 4.0 International License

1 Massive spectral data analysis for plant breeding using
2 parSketch-PLSDA method: discrimination of sunflower
3 genotypes

4 Maxime Ryckewaert^{a,b}, Maxime Metz^{a,b}, Daphné Héran^a, Pierre George^c,
5 Bruno Grèzes-Besse^c, Reza Akbarinia^d, Jean-Michel Roger^{a,b}, Ryad
6 Bendoula^a

7 ^a*ITAP, Univ Montpellier, INRAE, Institut Agro, Montpellier, France*

8 ^b*ChemHouse Research Group, Montpellier, France*

9 ^c*Innolea, 6 chemin des Panedautes, 31700 Mondonville, France*

10 ^d*Inria & LIRMM, Univ Montpellier, France*

11 Abstract

12 In precision agriculture and plant breeding, the amount of data tends to
13 increase. This massive data is becoming more and more complex, leading
14 to difficulties in managing and **analysing** it. Optical instruments such as
15 NIR Spectroscopy or hyperspectral imaging are gradually expanding directly
16 in the field, increasing the amount of spectral database. **Using these tools**
17 **allows access to non-destructive and rapid measurements to classify new va-**
18 **rieties according to breeding objectives.** Processing this massive amount of
19 spectral data is challenging. In a context of genotype discrimination, we pro-
20 pose to apply a method called parSketch-PLSDA to **analyse** such a massive
21 amount of spectral data. **ParSketch-PLSDA is a combination of an index-**
22 **ing strategy (parSketch) and the reference method (PLSDA) for predicting**
23 **classes from multivariate data.** For this purpose, a spectral database was
24 formed by collecting 1,300,000 spectra **generated from hyperspectral images**
25 **of leaves of four different sunflower genotypes.** ParSketch-PLSDA is com-

²⁶ pared to a PLSDA. Both methods use the same set of calibration and test.
²⁷ The prediction model obtained by PLSDA has a classification error close
²⁸ to 23% on average across all genotypes. ParSketch-PLSDA method outper-
²⁹ forms PLSDA by greatly improving prediction qualities by 10%. **Indeed, the**
³⁰ **model built with ParSketch-PLSDA has the ability to take into account non-**
³¹ **linearities among data sets.** These results are encouraging and allow us to
³² anticipate the future bottleneck related to the generation of a large amount
³³ of data from phenotyping.

³⁴ *Keywords:* Spectroscopy, Massive data, Digital Agriculture, Precision
³⁵ Agriculture, Chemometrics

³⁶ **1. Introduction**

³⁷ In recent years, precision agriculture and plant breeding have tended to
³⁸ increase the quantity and complexity of phenotyping related data ([Mahlein](#),
³⁹ [2016](#); [Tripodi et al., 2018](#); [Awada et al., 2018](#)). Managing and [analysing](#)
⁴⁰ huge amounts of data are identified as a future bottleneck in phenotyping
⁴¹ ([Tripodi et al., 2018](#)). Indeed, over the last few years, high throughput
⁴² phenotyping (HTP) platforms in the laboratory or directly in the field have
⁴³ been flourishing ([Chawade et al., 2019](#); [Shakoor et al., 2017](#)). These platforms
⁴⁴ provide a monitoring of one or more phenotypic traits of the vegetation. This
⁴⁵ information can be obtained at different spatial, spectral or temporal scales
⁴⁶ depending on the studied level, which could be vegetation organ, individual
⁴⁷ or even population ([Dhondt et al., 2013](#); [Mahlein, 2016](#); [Mutka et al., 2016](#)).
⁴⁸ The higher the spatial, spectral or temporal resolution, the larger the amount
⁴⁹ of data.

50 Spectroscopy in the visible and near-infrared range (VIS-NIR) has proven
51 to be relevant for providing useful information for vegetation monitoring.
52 Several plant phenotyping issues can be tackled with high spectral resolution
53 measurements such as biochemical variable access (Vigneau et al., 2011; Jay
54 et al., 2017), disease (Lu et al., 2018; Yu et al., 2018) or stress detection
55 (Behmann et al., 2014; Christensen et al., 2005).

56 From a technological point of view, spectral acquisitions directly in the
57 field have been made possible thanks to spectrometer **miniaturisation** (Yan
58 and Siesler, 2018; Beć et al., 2020) or hyperspectral imager evolution (Mishra
59 et al., 2020; Fiorani and Schurr, 2013). Associated with mobile vectors (such
60 as UAV, tractor, pedestrian), these tools become **HTP** instruments and gen-
61 erate a large amount of spectral data. However, simple computations on this
62 amount of data such as outlier detection or the use of pre-processing become
63 difficult to perform and very time consuming (Szymańska, 2018). Processing
64 this massive amount of spectral data is challenging.

65 In chemometrics, most popular methods as Partial Least Square (PLS)
66 (Wold et al., 2001) are based on an assumption of linear relationship be-
67 tween spectral data and specific variables (Mark and Workman, 2007). These
68 methods are popular because of their good predictive performances and low
69 computation time. Conversely, using these methods may not provide good
70 prediction models when relationships between spectra and variable of interest
71 are non-linear.

72 When dealing with a large amount of spectral data, complex structures
73 and non-linear relationships can arise which may compromise linear regres-
74 sion approaches (Dardenne et al., 2000). In practice, using a linear classifi-

75 cation or regression to predict a complex database would lead to degraded
76 results (Bertran et al., 1999; Ni et al., 2014). As a consequence, linear meth-
77 ods are challenged on large amounts of data. Furthermore, some methods,
78 called local methods, exploit data based on a restricted neighbourhood of
79 individuals which greatly improves prediction quality (Dardenne et al., 2000;
80 Pérez-Marín et al., 2007; Davrieux et al., 2016; Naes et al., 1990). These
81 methods can be used to overcome non-linearity problems under the assump-
82 tion that with a restricted neighbourhood, the relationship between spectra
83 and variables becomes linear. The parSketch-PLSDA method has recently
84 been proposed to implement a local approach to a large volume of data
85 (Metz et al., 2020). Therefore, parSketch-PLSDA can be used to address the
86 complex analysis of large amount of spectral data from phenotyping.

87 In this paper, we propose to study the use of the parSketch-PLSDA
88 method to exploit a large amount of spectral data, generated from hyper-
89 spectral images of leaves of four different sunflower genotypes. Additionally,
90 we compare this method with a reference method in an application of dis-
91 crimination of different sunflower varieties.

92 2. Materials and methods

93 2.1. Biological material

94 Four sunflower genotypes (called A, B, C and D) were grown in a green-
95 house at INRAE France in well-watered conditions by using a flood and
96 drain system refilling water every 48 hours. All pots used the same pot-
97 ting soil (Pot Clay coarse, Floradur, Floragard). Water and lighting con-
98 ditions were similar for each pot with a day-night cycle of 16h/8h. The

99 temperature was 25°C with a relative humidity in the greenhouse ranging
100 from 50% to 60%. The greenhouse was equipped with multispectral light-
101 ing (450 nm, 560 nm, 660 nm, 730 nm and 6000°K) controlled by Herbro
102 automaton (GreenHouseKeeper) with Photosynthetically Active Radiation
103 (PAR) set at 400 $\mu\text{mol}/\text{m}^2/\text{s}$.

104 For the four selected genotypes, two potted plants (called P1 and P2)
105 of each were grown. Four leaves were collected at the upper and middle
106 parts of each plant, except for the genotype D where only two leaves of each
107 plant were collected. Leaf petioles were immediately wrapped with water
108 soaked paper before measurements. In total, 28 leaves were then collected
109 and measured.

110 *2.2. Spectral acquisitions*

111 Spectral data of the prepared leaf samples were acquired in the reflectance
112 mode by using a laboratory-based line scanning Hyperspectral Imaging Sys-
113 tem (HIS). The HIS system was composed of a linear halogen light (Haloline,
114 Osram, 150 W), a translation rail (Linear Unit LES 4, Iselautomation, Ger-
115 many), and a detection system. The sample was placed on a translation
116 rail, synchronised with the acquisition software (NEO Hypspex, Norsk Elek-
117 tro Optikk AS) which can record images when sample was scanned under the
118 hyperspectral camera (NEO Hypspex VNIR-1600 with 30cm-objective, Norsk
119 Elektro Optikk AS, Skedsmokorest, Norway). Spectral data were acquired
120 in the 400 – 1000 nm wavelength range with 3.7 nm intervals.

121 For each sample, the reflected light intensity ($I_s(\lambda)$) was measured at
122 each wavelength . Dark current image ($I_b(\lambda)$) was also recorded for each
123 measure. A white reference (SRS99, Spectralon ®) was used as a reference

₁₂₄ ($I_o(\lambda)$) to standardize images from non-uniformities of all components of the
₁₂₅ instrumentation (light source, lens, detector). From these measurements,
₁₂₆ reflectance ($R_s(\lambda)$) was calculated for each sample:

$$R_s(\lambda) = \frac{I_s(\lambda) - I_b(\lambda)}{I_0(\lambda) - I_b(\lambda)} \quad (1)$$

₁₂₇ For all hyperspectral images, vegetation pixels were selected to form a
₁₂₈ spectral data set. This selection was made by a threshold **procedure** (Fig. 1).
₁₂₉ Indeed, vegetation and background pixels were easily identified by comparing
₁₃₀ their reflectance value at 800 nm to a threshold defined here at 30%. Leaf
₁₃₁ spectra were collected from the 28 hyperspectral images, representing more
₁₃₂ than 1,300,000 spectra.



Figure 1: Pixel selection from a hyperspectral image of a sunflower leaf (a) image, (b) mask based on threshold values

₁₃₃ *2.3. Data analysis*

₁₃₄ Two methods were used to compare their ability to discriminate sunflower
₁₃₅ genotypes. Both methods were applied to a similar data set, called test set,
₁₃₆ built out of the spectra database. Calculations were performed with the
₁₃₇ R software (version 3.6.1 (Core Team, 2013)) and rnirs package (<https://>

¹³⁸ github.com/mlesnoff/rnirs) was used for classical discrimination methods
¹³⁹ (PLSDA).

¹⁴⁰ *2.3.1. PLSDA method*

¹⁴¹ The Partial Least Squares for Discrimination Analysis (PLSDA) ([Barker](#)
¹⁴² [and Rayens, 2003](#)) was used as reference method for classification. This
¹⁴³ method consisted of building models between multivariate data and a vector
¹⁴⁴ coding different classes (here, the four genotypes).

¹⁴⁵ Multivariate data was represented by a matrix \mathbf{X} of size (n, p) where n
¹⁴⁶ was the observation number and p the variable number. The n observations
¹⁴⁷ were identified by their corresponding class in the vector y of size $(n, 1)$ where
¹⁴⁸ values ranged from 1 to q , where q was the class number. The first step was
¹⁴⁹ to transform y into a dummy matrix \mathbf{Y} of size (n, q) also called disjunctive
¹⁵⁰ table.

$$y = \begin{bmatrix} 1 \\ 1 \\ 1 \\ 2 \\ 2 \\ 2 \\ 3 \\ 3 \\ 3 \end{bmatrix} \rightarrow \mathbf{Y} = \begin{bmatrix} 1 & 0 & 0 \\ 1 & 0 & 0 \\ 1 & 0 & 0 \\ 0 & 1 & 0 \\ 0 & 1 & 0 \\ 0 & 1 & 0 \\ 0 & 0 & 1 \\ 0 & 0 & 1 \\ 0 & 0 & 1 \end{bmatrix} \quad (2)$$

¹⁵¹ An example of a dummy matrix is given in equation 2 with nine observa-
¹⁵² tions belonging to three classes. The matrix \mathbf{Y} contains binary values (0,1)

153 where each column corresponded to a class. For a given observation, the
154 class-corresponding column has a value of 1 while other columns were equal
155 to 0.

156 Then, a Partial Least Square (PLS) model (Wold et al., 2001) was applied
157 between \mathbf{X} and \mathbf{Y} . \mathbf{Y} being multidimensional, the algorithm PLS2 adapted
158 to the prediction of several responses was used. Finally, a linear discriminant
159 analysis (LDA) (Fisher, 1936) was applied between the PLS2 scores and \mathbf{Y} .

160 *2.3.2. ParSketch-PLSDA method*

161 The other strategy was to apply the parSketch-PLSDA method (Metz
162 et al., 2020), an extension of the K-Nearest Neighbours (KNN)-PLSDA
163 method for massive data processing (Lesnoff et al., 2020). ParSketch-PLSDA
164 was used to combine an indexation strategy (parSketch) and the PLSDA.
165 An approximation of the neighbourhood was defined for each spectrum to be
166 classified. This neighbourhood was then used to compute a PLSDA model
167 and to predict which class belong new spectra.

168 ParSketch was performed in three steps: dimension reduction, grid cre-
169 ation, neighbourhood approximation. Three method parameters (v , s , m)
170 were defined, corresponding to these three steps, and are described below.

171 First, a dimension reduction was achieved by calculating the matrix \mathbf{T}
172 corresponding to the sketch of the matrix \mathbf{X} as follows:

$$\mathbf{T} = \mathbf{XP} \quad (3)$$

173 Where \mathbf{P} was a matrix of size (p, v) containing values of -1 or 1 according
174 to a random selection. The first parameter of ParSketch (v), corresponding
175 to the column number of \mathbf{P} was then defined. The higher the value of v

¹⁷⁶ the better the approximation of the **neighbourhood**. However, the larger the
¹⁷⁷ value of v the longer the parSketch method computation time.

¹⁷⁸ The second step corresponding to the grid creation process (see Fig. 2)
¹⁷⁹ was to segment the space (2d) formed by adjacent pairs of \mathbf{T} columns. The
¹⁸⁰ number of segments (s) is the second parSketch parameter. The higher the
¹⁸¹ value of s the better the approximation of the nearest **neighbours**. However,
¹⁸² the greater the value of s , the smaller the number of **neighbours**.

¹⁸³

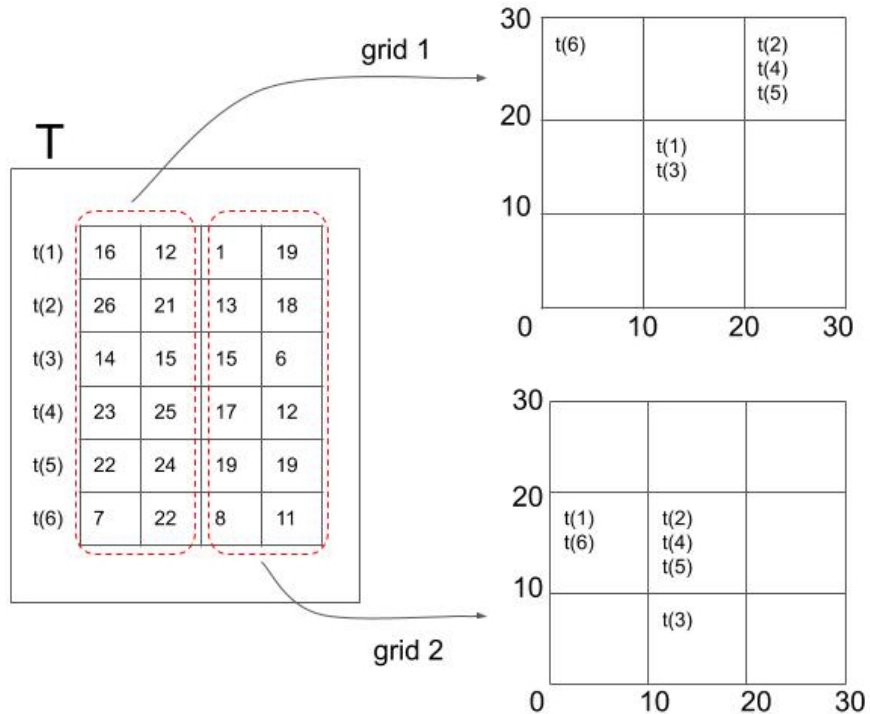


Figure 2: An illustrated example of grid creation with a segment number $s = 3$

¹⁸⁴ The last step to configure parSketch was to define the minimal number
¹⁸⁵ m of grids returned in the **neighbour**'s search. This step corresponded to the

186 neighbourhood approximation for the grid search process (see Fig. 3). The
 187 higher the value of m the better the approximation of the nearest neighbours.
 188 Observations present in the same cell for at least m grid number are selected
 189 as neighbours of the individual to be predicted. However, the greater the
 190 value of m , the smaller the number of neighbours returned by parSketch
 191 method.

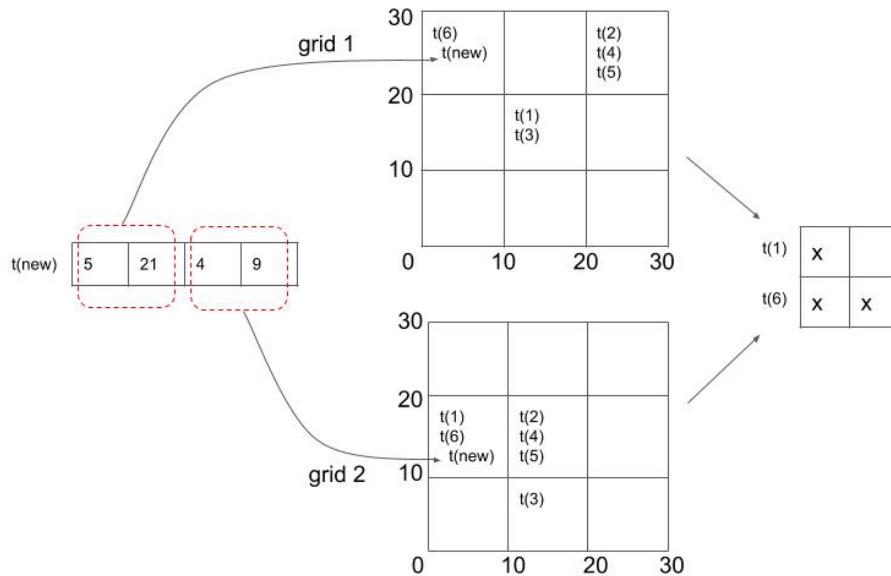


Figure 3: An illustrated example of grid search. For a new measure $t(\text{new})$ and a m value equals to 2, $t(6)$ will be returned as a neighbour because it is present in two grids next to $t(\text{new})$, whereas $t(1)$ will not be considered as a neighbour

192 2.4. Evaluation strategies and method parameterization

193 The data set was divided into two independent data sets: a calibration
 194 set and an independent test set . The calibration set was formed with the
 195 14 images acquired on P1 plants and corresponding to about 650,000 spec-

196 tra. The PLSDA model and parSketch-PLSDA method were both calibrated
197 using all spectra of this calibration set.

198 The test set was formed with the other 14 images acquired on P2 plants
199 (independent from P1). 1000 spectra were randomly selected in each image
200 totalling 14,000 spectra for the test set. Spectra that could not be predicted
201 by parSketch due to lack of **neighbours** were removed from the test set. In
202 the end, the same test set were used for parSketch-PLSDA and for PLSDA.

203 For both methods, validation steps were performed on the calibration set
204 in order to minimize overfitting.

205 To build the PLSDA model, the cross-validation step consisted of splitting
206 the calibration data set into different blocks in order to calculate calibration
207 and validation errors. This approach, also called k-fold validation ([Wold, 1978](#);
[Camacho and Ferrer, 2012](#)) was carried out with five blocks repeated
208 three times. Validation errors were then computed and led to the number of
209 latent variables to be retained.

210 For parSketch-PLSDA, a parametrisation step was performed to config-
211 ure the three parSketch parameters. This step was performed by analyzing
212 distributions of returned **neighbours** according to two parSketch parameters:
213 number of segments s and the common minimum grids m . Here, the number
214 of random vectors v was set to a value of 20. Afterwards, a PLSDA model
215 was established. The number of latent variables was optimized for a subset of
216 the calibration set, called the validation set. This validation set was formed
217 with four images of the calibration set by randomly selecting 1000 spectra in
218 each image.

219 In order to compare both methods, confusion matrices were obtained and

221 percentages of precision and recall were calculated according to the following
222 equations:

$$\text{Precision} = \frac{tp}{tp + fp} \quad (4)$$

$$\text{Recall} = \frac{tp}{tp + fn} \quad (5)$$

223 Where tp , fp and fn corresponded to true positives, false positives and
224 false negatives respectively. On the one hand, for a given class, precision
225 value assessed the predictive quality of the model based on the proportion
226 of well-classified observations among all observations that were classified in
227 the same corresponding class. On the other hand, recall, also called sensi-
228 tivity, evaluated the number of well-classified observations compared to the
229 total number of observations of the given class. These two criteria are com-
230 plementary to evaluate the model performances. These two figures of merit
231 were expressed as percentages. The higher the values, the better the model
232 performance.

233 **3. Results and discussion**

234 *3.1. Data visualization*

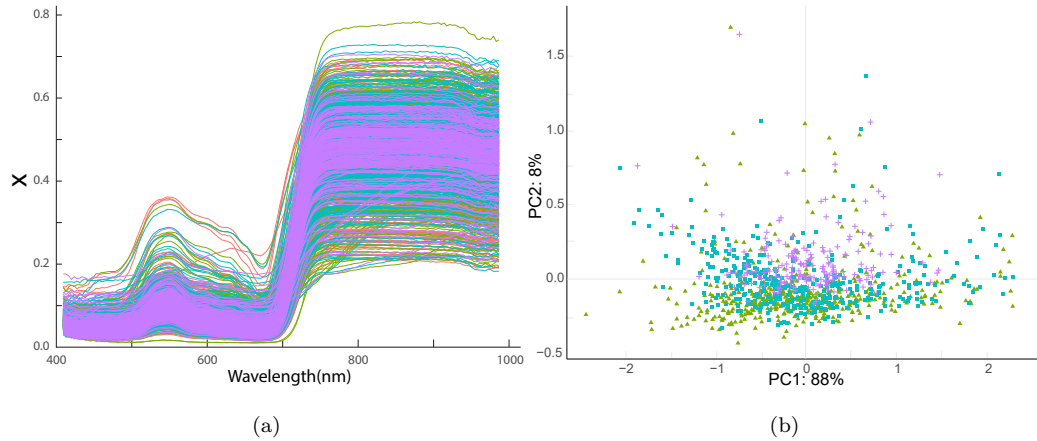


Figure 4: All data set including Genotype A (red), B (green), C (cyan) and D (violet):
 (a) spectra, (b) score plot of the first two principal components

235 Reflectance spectra shown in Fig. 4a correspond to 1000 spectra per
 236 class randomly selected among all the data set. These spectra correspond
 237 to vegetation spectra (Xu et al., 2019) : specific hollows at 450 nm and
 238 650 nm related to chlorophyll content, anthocyanin content at 550 nm; the
 239 red-edge towards 780 nm and a plateau in the near-infrared between 780 nm
 240 and 1000 nm. Besides, the main observed variability in the spectrum plot
 241 corresponds to an additive effect due to the scattering effect of the structure
 242 of the leaves. However, the number of spectra is too large to be able to
 243 describe difference between classes.

244 A principal component analysis was applied to these spectra. Figure 4b
 245 shows the score plot of the two first components. The first component rep-
 246 resents 88% of the spectra variability and 8% for the second component. On

247 these two components, scores are uniformly distributed without any evident
248 distinction between genotypes. The exploratory study of the spectra shows
249 that there are no outliers and that there is no distinct group on the first two
250 components.

251 *3.2. Model calibration*

252 *3.2.1. PLSDA*

253 Figure 5 shows the cross-validated error rate curve for PLSDA applied to
254 all spectra of the calibration data set. The behaviour of the curve decreases
255 continuously according to the latent variable (LV) number.

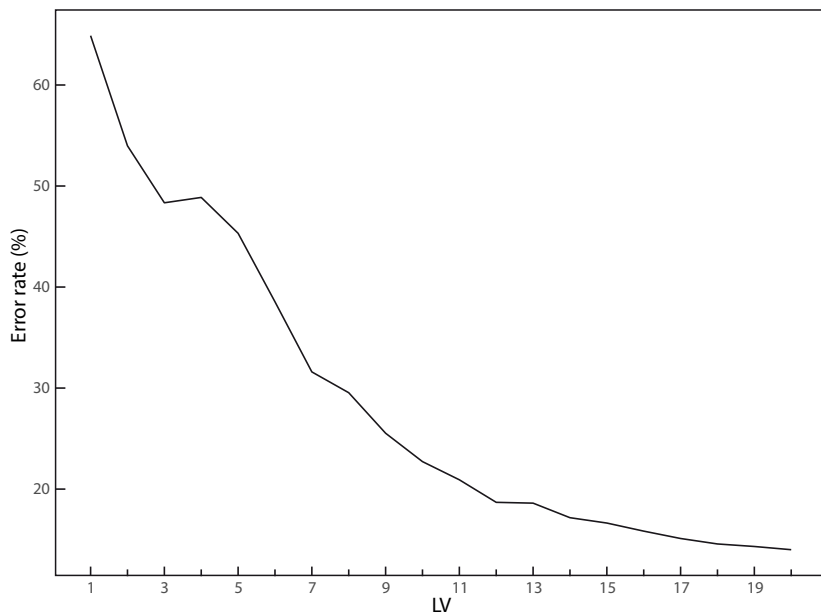


Figure 5: Evolution of the cross-validated error rate as a function of latent variables (LV)
for the PLSDA applied to all spectra of the calibration data set

256 A high value of LV number generally shows the complex structure of a
257 data set. This is expected with spectral measurements on vegetation ([Metz](#)

258 et al., 2020). With 16 LVs, an error rate with a value close to 12% is ob-
 259 tained. However, after 16 LVs the predictive performance gain is very small.
 260 Consequently, the PLSDA model is set to 16 LVs.

261 *3.2.2. ParSketch-PLSDA*

262 ParSketch parameters s and m are studied according to the statistical
 263 distribution of the number of returned neighbours (Fig. 6).

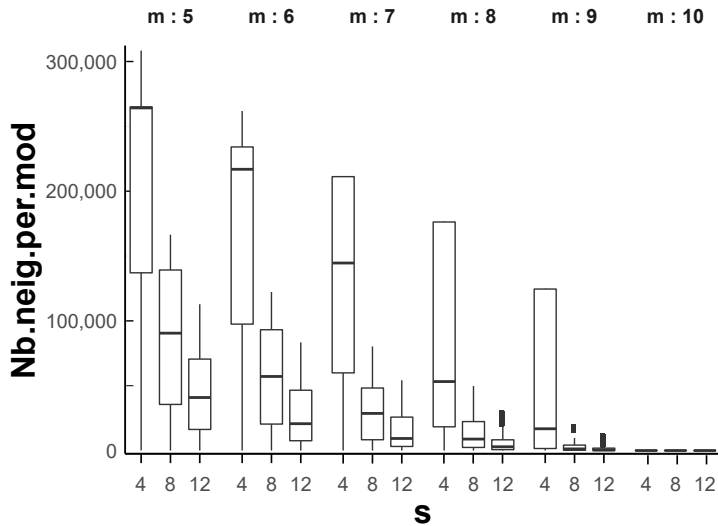


Figure 6: Distribution of the returned neighbours according to parSketch parameters s and m (number of segments and common minimum grids). Here, v (number of random vectors) parameter is fixed to 20

264 The number of neighbours decreases to a value close to zero when param-
 265 eter values (s,m) increase. Indeed, on the one hand, an increase of number
 266 of segments s , the number of returned neighbours will be lower. And on the
 267 other hand, by increasing the minimum number of common grids m , the risk
 268 of not having neighbours is high. This global trend is expected (Metz et al.,

269 2020).

270 By contrast, when parameter values are low, the number of returned
271 **neighbours** is high (close to 300 000 **neighbours** by individual to be pre-
272 dicted). This situation is not desirable, as it may cause problems related
273 to computation time constraints. As a result, parameters m and s must
274 be chosen to have a sufficient number of **neighbours**, neither too much nor
275 too little. As several values are possible, four combinations of the parSketch
276 parameters are selected (Table 1) to compare their model performances.

Table 1: Combinations of the selected parSketch parameters and the corresponding median number of returned **neighbours**

Combination	m	v	s	Median neighbour number
(a)	9	20	8	1246
(b)	8	20	12	2903
(c)	7	20	12	9303
(d)	6	20	12	27030

277 Table 1 shows the retained values of the three parSketch parameters for
278 these four combinations. The combination (a) was selected because the
279 median number of **neighbours** is 1246. This low number of **neighbours** enables
280 to quickly calibrate PLSDA models but it could be insufficient to have a
281 good predictive quality. Indeed, a low median number of **neighbours** means
282 that a large amount of observations do not have **neighbour** at all. For the
283 combinations (b) and (c), higher numbers of **neighbours** are returned, with
284 median values of 2903 and 9303 respectively. Finally, the highest median
285 number of **neighbours** returned by parSketch is chosen with the combination

286 (d) with a value equal to 27030. In this case, constraints in computation
287 time might appear. Moreover, the linear relationship between spectra and
288 class variable of a small **neighbourhood** might be lost.

289 Validation error curves for the four retained combinations for parSketch-
290 PLSDA are shown in the figure 7.

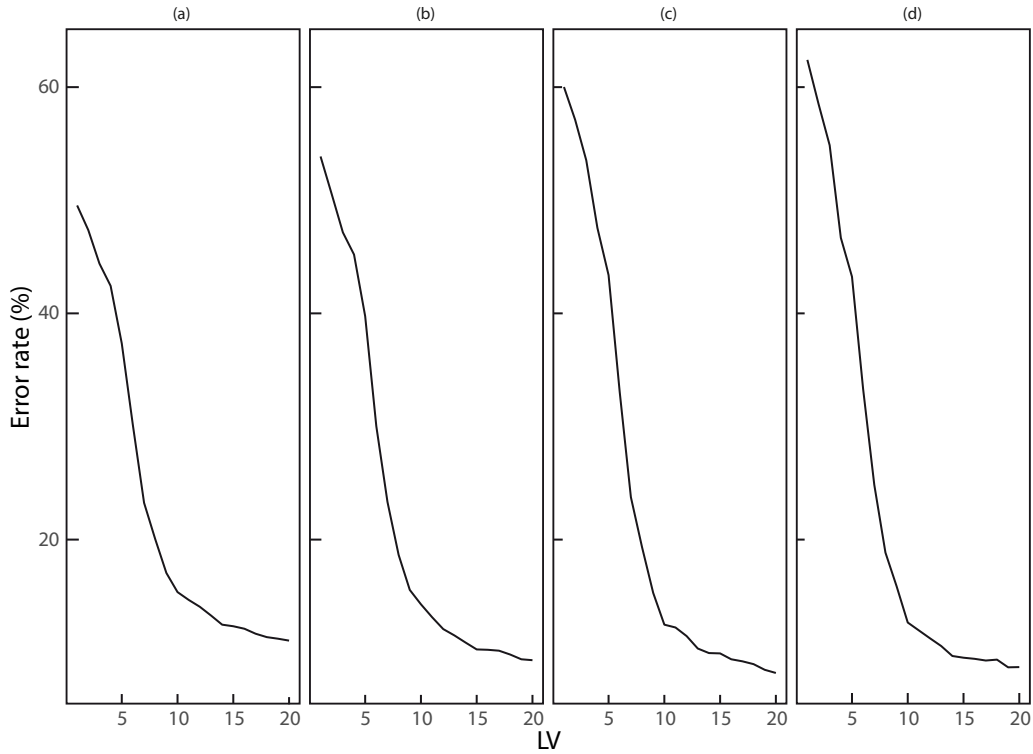


Figure 7: Evolution of the validation error rate as a function of latent variables for the four parameter combinations of parSketch-PLSDA

291 With higher error values, the combination (a) is less predictive than
292 other parameter combinations. As expected, this combination having the
293 smallest number of **neighbours**, the resultant model has poorer predictive
294 performances than the three other ones.

295 The error curve obtained with the combination **(b)** reaches lower rates
296 than the combination **(a)** curve. This means that the predictive capabilities
297 of the model can be improved by slightly increasing the number of **neighbours**.
298 The combination **(c)** has best predictive performance for the validation set
299 with lowest values of classification error. The combination **(d)** has lower
300 prediction quality than the combination **(c)** for a larger median number of
301 **neighbours** per sample to be predicted (cf. Table 1).

302 The model with the lowest predictive quality has a high number of **neigh-**
303 **bours**. This degradation reflects a non-linear aspect of the data set. By
304 further increasing the number of returned **neighbours**, prediction qualities of
305 parSketch will be close to the PLSDA method on the whole data set.

306 Finally, for this validation set the optimal parameter combination is the
307 combination **(c)**. In this case, the number of latent variables is not easy to
308 define. The number of latent variables is defined by a trade-off between the
309 size of the model and the benefit of adding an extra dimension to the model.

310 The number of latent variables chosen is therefore 16.

311 *3.3. Model testing*

312 The PLSDA model has been calibrated with all the spectra of the cali-
313 bration set. Then this model is applied to the test set defined previously and
314 its prediction performances are assessed in Table 2.

Table 2: Confusion matrix for PLSDA (16 LVs)

	A	B	C	D	Recall (%)
A	3120	121	339	250	81
B	238	2812	619	154	74
C	127	241	3463	75	89
D	283	173	270	1213	63
Precision(%)	83	84	74	72	

315 Precision and recall values are high for all classes A, B, C and D with
 316 values ranging from 72% to 84% for precision and from 63% to 89% for
 317 recall. Genotypes A and B have the highest precision values with values of
 318 83% and 84%, respectively. This means that 83% of spectra classified in
 319 genotype A, actually belong to genotype A. Few other genotypes are found
 320 in this class. The same argumentation holds true for 84% of genotype B
 321 spectra. For recall, genotypes A and C have the best values with 81% and
 322 89%, respectively. For these genotypes, spectra are mainly well-classified
 323 that is infrequently assigned to other classes.

324 The percentage missings from recall values correspond to the prediction
 325 error for each class. The prediction error of the whole data set, corresponding
 326 to the average error, is close to 23%. It is expected to have value for the test
 327 error slightly higher than the 12% observed during calibration (see Fig. 5).
 328 This means that the calibration set samples are representative of the test set
 329 despite their independence (as mentioned above, the test set corresponds to
 330 other plants of the same genotype).

Table 3: Confusion matrix for parSketch-PLSDA with combination(**c**) ($m = 7$, $v = 20$, $s = 12$)

	A	B	C	D	Recall (%)
A	3547	114	115	54	93
B	40	3256	473	54	85
C	58	211	3590	47	92
D	51	112	260	1516	78
Precision(%)	96	88	81	91	

331 Table 3 shows the parSketch-PLSDA prediction performance by giving
 332 percentages of precision and recall for each genotype. Genotypes A and D
 333 have the highest precision values with values of 96% and 91% respectively.
 334 Besides, genotypes A and C have the highest recall values with values of
 335 93% and 92% respectively. Genotype D has low recall values with both
 336 methods (63% for PLSDA and 78% for parSketch-PLSDA). This is probably
 337 due to the under-representation in the data set which may degrade the model
 338 calibration. Indeed, only two images were acquired per plant of genotype D
 339 compared to four images for the other genotypes.

340 Finally, overall recall and precision values have increased by almost 10%
 341 with parSketch-PLSDA (**83%** and **87%** respectively) compared to PLSDA
 342 (**76%** and **77%** respectively). Consequently, the model prediction error de-
 343 creases to a value of 13%. This implies that parSketch-PLSDA model per-
 344 forms better than the reference discriminant strategy. This improvement
 345 in the classification results demonstrates the advantage of using a limited
 346 number of **neighbours** to create a model.

347 As the methods used are locally linear, this improvement confirms the hy-
348 pothesis that with a limited number of **neighbours**, the problem becomes lin-
349 ear. The prediction improvement obtained with parSketch-PLSDA method
350 highlights the presence of non-linear relationships between spectra and a class
351 variable in the whole data set. which can be encountered when building a
352 large spectral database.

353 4. Conclusion

354 In this study, we compared the two classification strategies on the same
355 calibration and test data sets.

356 For both methods, classification results are encouraging and confirm the
357 interest of VIS-NIR spectroscopy for variety discrimination. Results showed
358 that parSketch-PLSDA method outperforms PLSDA by improving predic-
359 tion qualities by 10%. The use of the parSketch-PLSDA procedure in the
360 exploitation of massive spectral data is confirmed and shows the interest of
361 using a close **neighbourhood** of the spectra to be predicted.

362 It would be interesting to test such methods on a larger number of geno-
363 types. This increase in the spectral database can potentially lead to an
364 increase in complexity hence reducing the data set quality. Therefore, it
365 would be interesting, in perspective, to evaluate other methods dealing with
366 non-linearity.

367 In the framework of plant breeding, hyperspectral imaging or field mi-
368 crospectrometers as tools for high-throughput plant phenotyping could be
369 considered in real time with this method. In an applicative aspect, parS-
370 ketch procedure is **parallelisable**, which shows the possibility of fast real-time

371 prediction of a large amount of data. We used parSketch-PLSDA on spectral
372 data for close-range plant phenotyping. Other applications to plant breed-
373 ing (disease, biotic/abiotic stress) or other applications related to precision
374 agriculture could be considered. More generally, this method can be applied
375 to any other application in analytical chemistry or metabolomics.

376 **Acknowledgement**

377 This work was conducted within the OPTIPAG Project supported by the
378 grant ANR-16-CE04-0010 from the French Agence Nationale de la Recherche.

379 **References**

- 380 Anne-Katrin Mahlein. Plant disease detection by imaging sensors—parallels
381 and specific demands for precision agriculture and plant phenotyping.
382 *Plant disease*, 100(2):241–251, 2016. Publisher: Am Phytopath Society.
- 383 Pasquale Tripodi, Daniele Massa, Accursio Venezia, and Teodoro Cardi.
384 Sensing technologies for precision phenotyping in vegetable crops: cur-
385 rent status and future challenges. *Agronomy*, 8(4):57, 2018. Publisher:
386 Multidisciplinary Digital Publishing Institute.
- 387 Lana Awada, Peter W. B. Phillips, and Stuart J. Smyth. The adoption of
388 automated phenotyping by plant breeders. *Euphytica*, 214(8):148, August
389 2018. ISSN 0014-2336, 1573-5060. doi: 10.1007/s10681-018-2226-z. URL
390 <http://link.springer.com/10.1007/s10681-018-2226-z>.
- 391 Aakash Chawade, Joost van Ham, Hanna Blomquist, Oscar Bagge, Erik
392 Alexandersson, and Rodomiro Ortiz. High-throughput field-phenotyping

- 393 tools for plant breeding and precision agriculture. *Agronomy*, 9(5):258,
394 2019. Publisher: Multidisciplinary Digital Publishing Institute.
- 395 Nadia Shakoor, Scott Lee, and Todd C. Mockler. High throughput pheno-
396 typing to accelerate crop breeding and monitoring of diseases in the field.
397 *Current opinion in plant biology*, 38:184–192, 2017. Publisher: Elsevier.
- 398 Stijn Dhondt, Nathalie Wuyts, and Dirk Inzé. Cell to whole-plant phe-
399 nototyping: the best is yet to come. *Trends in Plant Science*, 18(8):
400 428–439, August 2013. ISSN 1360-1385. doi: 10.1016/j.tplants.2013.
401 04.008. URL <http://www.sciencedirect.com/science/article/pii/S1360138513000812>.
- 402
- 403 Andrew M. Mutka, Sarah J. Fentress, Joel W. Sher, Jeffrey C. Berry,
404 Chelsea Pretz, Dmitri A. Nusinow, and Rebecca Bart. Quantitative,
405 image-based phenotyping methods provide insight into spatial and tem-
406 poral dimensions of plant disease. *Plant Physiology*, page pp.00984.2016,
407 July 2016. ISSN 0032-0889, 1532-2548. doi: 10.1104/pp.16.00984. URL
408 <http://www.plantphysiol.org/lookup/doi/10.1104/pp.16.00984>.
- 409
- 410 Nathalie Vigneau, Martin Ecarot, Gilles Rabatel, and Pierre Roumet. Po-
411 tential of field hyperspectral imaging as a non destructive method to as-
412 sess leaf nitrogen content in wheat. *Field Crops Research*, 122(1):25–31,
413 April 2011. ISSN 03784290. doi: 10.1016/j.fcr.2011.02.003. URL <http://linkinghub.elsevier.com/retrieve/pii/S0378429011000451>.
- 414
- 415 Sylvain Jay, Nathalie Gorretta, Julien Morel, Fabienne Maupas, Ryad Ben-
doula, Gilles Rabatel, Dan Dutartre, Alexis Comar, and Frédéric Baret.

- 416 Estimating leaf chlorophyll content in sugar beet canopies using millimeter-
417 to centimeter-scale reflectance imagery. *Remote Sensing of Environment*,
418 198:173–186, 2017. Publisher: Elsevier.
- 419 Jinzhu Lu, Reza Ehsani, Yeyin Shi, Ana Isabel de Castro, and Shuang
420 Wang. Detection of multi-tomato leaf diseases (late blight , target
421 and bacterial spots) in different stages by using a spectral-based sen-
422 sor. *Scientific Reports*, 8(1):2793, February 2018. ISSN 2045-2322. doi:
423 10.1038/s41598-018-21191-6. URL <https://www.nature.com/articles/s41598-018-21191-6>. Number: 1 Publisher: Nature Publishing Group.
- 425 Kang Yu, Jonas Anderegg, Alexey Mikaberidze, Petteri Karisto, Fabio
426 Mascher, Bruce A. McDonald, Achim Walter, and Andreas Hund. Hyper-
427 spectral Canopy Sensing of Wheat Septoria Tritici Blotch Disease. *Fron-*
428 *tiers in Plant Science*, 9, 2018. ISSN 1664-462X. doi: 10.3389/fpls.2018.
429 01195. URL <https://www.frontiersin.org/articles/10.3389/fpls.2018.01195/full>. Publisher: Frontiers.
- 431 Jan Behmann, Jörg Steinrücken, and Lutz Plümer. Detection of early
432 plant stress responses in hyperspectral images. *ISPRS Journal of Pho-*
433 *togrammetry and Remote Sensing*, 93:98–111, 2014. URL <http://www.sciencedirect.com/science/article/pii/S092427161400094X>.
- 435 Lene K. Christensen, Shrinivasa K. Upadhyaya, Bernie Jahn, David C.
436 Slaughter, Eunice Tan, and David Hills. Determining the Influence of
437 Water Deficiency on NPK Stress Discrimination in Maize using Spec-
438 tral and Spatial Information. *Precision Agriculture*, 6(6):539–550, De-

- 439 cember 2005. ISSN 1573-1618. doi: 10.1007/s11119-005-5643-7. URL
440 <https://doi.org/10.1007/s11119-005-5643-7>.
- 441 Hui Yan and Heinz W. Siesler. Hand-held near-infrared spectrometers: State-
442 of-the-art instrumentation and practical applications. *NIR news*, 29(7):
443 8–12, 2018. Publisher: SAGE Publications Sage UK: London, England.
- 444 Krzysztof B. Beć, Justyna Grabska, Heinz W. Siesler, and Christian W. Huck.
445 Handheld near-infrared spectrometers: Where are we heading? *NIR news*,
446 31(3-4):28–35, 2020. Publisher: SAGE Publications Sage UK: London,
447 England.
- 448 Puneet Mishra, Santosh Lohumi, Haris Ahmad Khan, and Alison Nor-
449 don. Close-range hyperspectral imaging of whole plants for digital phe-
450 nototyping: Recent applications and illumination correction approaches.
451 *Computers and Electronics in Agriculture*, 178:105780, November 2020.
452 ISSN 01681699. doi: 10.1016/j.compag.2020.105780. URL <https://linkinghub.elsevier.com/retrieve/pii/S016816992031869X>.
- 454 Fabio Fiorani and Ulrich Schurr. Future Scenarios for Plant Phenotyping.
455 *Annual Review of Plant Biology*, 64(1):267–291, April 2013. ISSN
456 1543-5008, 1545-2123. doi: 10.1146/annurev-arplant-050312-120137.
457 URL <http://www.annualreviews.org/doi/abs/10.1146/annurev-arplant-050312-120137>.
- 459 Ewa Szymańska. Modern data science for analytical chemical data – A com-
460 prehensive review. *Analytica Chimica Acta*, 1028:1–10, October 2018.

- 461 ISSN 0003-2670. doi: 10.1016/j.aca.2018.05.038. URL <http://www.sciencedirect.com/science/article/pii/S0003267018306421>.
- 463 Svante Wold, Michael Sjöström, and Lennart Eriksson. PLS-regression: a ba-
464 sic tool of chemometrics. *Chemometrics and intelligent laboratory systems*,
465 58(2):109–130, 2001.
- 466 Howard Mark and Jerry Workman. *Chemometrics in spectroscopy*. Else-
467 vier/Academic Press, Amsterdam, 2007. ISBN 978-0-12-374024-3. OCLC:
468 255877127.
- 469 Pierre Dardenne, George Sinnaeve, and Vincent Baeten. Multivariate
470 Calibration and Chemometrics for near Infrared Spectroscopy: Which
471 Method? *Journal of Near Infrared Spectroscopy*, 8(4):229–237, Octo-
472 ber 2000. ISSN 0967-0335, 1751-6552. doi: 10.1255/jnirs.283. URL
473 <http://journals.sagepub.com/doi/10.1255/jnirs.283>.
- 474 E. Bertran, M. Blanco, S. MasPOCH, M. C. Ortiz, M. S. Sánchez, and
475 L. A. Sarabia. Handling intrinsic non-linearity in near-infrared reflectance
476 spectroscopy. *Chemometrics and Intelligent Laboratory Systems*, 49(2):
477 215–224, October 1999. ISSN 0169-7439. doi: 10.1016/S0169-7439(99)
478 00043-X. URL <http://www.sciencedirect.com/science/article/pii/S016974399900043X>.
- 480 Wangdong Ni, Lars Nørgaard, and Morten Mørup. Non-linear calibra-
481 tion models for near infrared spectroscopy. *Analytica Chimica Acta*,
482 813:1–14, February 2014. ISSN 0003-2670. doi: 10.1016/j.aca.2013.

- 483 12.002. URL <http://www.sciencedirect.com/science/article/pii/S0003267013015158>.
- 484
- 485 D. Pérez-Marín, A. Garrido-Varo, and J. E. Guerrero. Non-linear regression
486 methods in NIRS quantitative analysis. *Talanta*, 72(1):28–42, April 2007.
487 ISSN 0039-9140. doi: 10.1016/j.talanta.2006.10.036. URL <http://www.sciencedirect.com/science/article/pii/S0039914006007119>.
- 488
- 489 F. Davrieux, D. Dufour, P. Dardenne, J. Belalcazar, M. Pizarro, J. Luna,
490 L. Londoño, A. Jaramillo, T. Sanchez, N. Morante, F. Calle, L.A. Be-
491 cerra Lopez-Lavalle, and H. Ceballos. LOCAL Regression Algorithm
492 Improves near Infrared Spectroscopy Predictions When the Target Con-
493 stituent Evolves in Breeding Populations. *Journal of Near Infrared Spec-*
494 *troscopy*, 24(2):109–117, April 2016. ISSN 0967-0335, 1751-6552. doi:
495 10.1255/jnirs.1213. URL <http://journals.sagepub.com/doi/10.1255/jnirs.1213>.
- 496
- 497 Tormod. Naes, Tomas. Isaksson, and Bruce. Kowalski. Locally weighted
498 regression and scatter correction for near-infrared reflectance data. *Ana-*
499 *lytical Chemistry*, 62(7):664–673, April 1990. ISSN 0003-2700, 1520-6882.
500 doi: 10.1021/ac00206a003. URL <https://pubs.acs.org/doi/abs/10.1021/ac00206a003>.
- 501
- 502 Maxime Metz, Matthieu Lesnoff, Florent Abdelghafour, Reza Akbarinia,
503 Florent Masseglia, and Jean-Michel Roger. A “big-data” algorithm
504 for KNN-PLS. *Chemometrics and Intelligent Laboratory Systems*, 203:
505 104076, August 2020. ISSN 0169-7439. doi: 10.1016/j.chemolab.2020.

- 506 104076. URL <http://www.sciencedirect.com/science/article/pii/S0169743920301908>.
- 507
- 508 R. Core Team. R: A language and environment for statistical computing.
- 509 Vienna, Austria: R Foundation for Statistical Computing. *Available*, 2013.
- 510 Matthew Barker and William Rayens. Partial least squares for discrimina-
- 511 tion. *Journal of Chemometrics*, 17(3):166–173, March 2003. ISSN 0886-
- 512 9383, 1099-128X. doi: 10.1002/cem.785. URL <http://doi.wiley.com/10.1002/cem.785>.
- 513
- 514 R. A. Fisher. The Use of Multiple Measurements in Taxonomic Problems.
- 515 *Annals of Eugenics*, 7(2):179–188, 1936. ISSN 2050-1439. doi: <https://doi.org/10.1111/j.1469-1809.1936.tb02137.x>. URL <https://onlinelibrary.wiley.com/doi/abs/10.1111/j.1469-1809.1936.tb02137.x>.
- 516
- 517
- 518 _eprint: <https://onlinelibrary.wiley.com/doi/pdf/10.1111/j.1469-1809.1936.tb02137.x>.
- 519
- 520 Matthieu Lesnoff, Maxime Metz, and Jean-Michel Roger. Comparison of
- 521 locally weighted PLS strategies for regression and discrimination on agro-
- 522 nomic NIR data. *Journal of Chemometrics*, page 13, 2020.
- 523 Svante Wold. Cross-Validatory Estimation of the Number of Components
- 524 in Factor and Principal Components Models. *Technometrics*, 20(4):397–
- 525 405, 1978. ISSN 0040-1706. doi: 10.2307/1267639. Publisher: [Taylor
- 526 & Francis, Ltd., American Statistical Association, American Society for
- 527 Quality].

- 528 José Camacho and Alberto Ferrer. Cross-validation in PCA mod-
529 els with the element-wise k-fold (ekf) algorithm: theoretical as-
530 pects. *Journal of Chemometrics*, 26(7):361–373, 2012. ISSN
531 1099-128X. doi: <https://doi.org/10.1002/cem.2440>. URL <https://onlinelibrary.wiley.com/doi/abs/10.1002/cem.2440>. eprint:
532 <https://onlinelibrary.wiley.com/doi/pdf/10.1002/cem.2440>.
- 534 Jun-Li Xu, Alexia Gobrecht, Daphné Héran, Nathalie Gorretta, Marie
535 Coque, Aoife A. Gowen, Ryad Bendoula, and Da-Wen Sun. A polar-
536 ized hyperspectral imaging system for in vivo detection: Multiple applica-
537 tions in sunflower leaf analysis. *Computers and Electronics in Agriculture*,
538 158:258–270, March 2019. ISSN 0168-1699. doi: 10.1016/j.compag.2019.
539 02.008. URL <http://www.sciencedirect.com/science/article/pii/S0168169918314455>.
- 540